



HAL
open science

Infrared emission measurements of a recombining CO₂ plasma

Corentin H C Grimaldi, Sean D Mcguire, Christophe O Laux

► **To cite this version:**

Corentin H C Grimaldi, Sean D Mcguire, Christophe O Laux. Infrared emission measurements of a recombining CO₂ plasma. AIAA Scitech 2022 Forum, Jan 2022, San Diego, CA, United States. pp.1782, 10.2514/6.2022-1782 . hal-04559004

HAL Id: hal-04559004

<https://hal.science/hal-04559004v1>

Submitted on 25 Apr 2024

HAL is a multi-disciplinary open access archive for the deposit and dissemination of scientific research documents, whether they are published or not. The documents may come from teaching and research institutions in France or abroad, or from public or private research centers.

L'archive ouverte pluridisciplinaire **HAL**, est destinée au dépôt et à la diffusion de documents scientifiques de niveau recherche, publiés ou non, émanant des établissements d'enseignement et de recherche français ou étrangers, des laboratoires publics ou privés.

Infrared emission measurements of a recombining CO₂ plasma

Corentin H. C. Grimaldi¹, Sean D. McGuire² and Christophe O. Laux³
Laboratoire EM2C, CNRS UPR288, CentraleSupélec, Université Paris-Saclay, 3 rue Joliot Curie, 91190 Gif-sur-Yvette, France

Infrared emission measurements from a high temperature CO₂/Ar plasma are presented. An inductively coupled plasma torch was used to produce a CO₂/Ar plasma jet at atmospheric pressure. The plasma jet is initially close to Local Thermodynamic Equilibrium conditions at a temperature of 6650 K. This plasma is then passed at high velocity through a water-cooled test-section that forces rapid cooling and recombination. The subsequent thermochemical evolution of the plasma as it traverses the water-cooled tube is studied using Optical Emission Spectroscopy in the infrared region between 4.1 and 5.6 μm . The measured spectra at the exit of the torch and at the exit of the 35-cm test-section are calibrated in absolute intensity and compared with calculations done using the RADIS line-by-line radiation code. The measurements presented here are meant to provide a test case for comparison with kinetic modeling and/or CFD predictions.

I. Introduction

The entry of a capsule into the atmosphere of a planet or a satellite occurs at hypersonic velocities. The resulting shock wave that forms in front of the vehicle heats the surrounding gas and forms a plasma in the post-shock region. The study of the resulting convective and radiative heat fluxes to the capsule surface is critical for the design of the thermal protective system [1]. For Mars entry scenarios, where CO₂ represents 96% of the atmosphere [2], the radiative heat flux to the afterbody suffers from large uncertainties - up to 260% [3]. The rapid hydrodynamic expansion of the plasma into the afterbody region results in rapid cooling, chemical recombination, and a departure from equilibrium [4]. This chemical non-equilibrium and the associated radiation are still not accurately modeled, and our goal is to provide experimental data for model validation as part of an effort to help reduce this uncertainty. Our experiments focus on a fundamental study of the recombination kinetics of CO₂ plasmas [5]. For these experiments, the plasma is first created by an inductively coupled plasma torch facility. The plasma is then passed through a water-cooled tube at high speed to force rapid cooling and chemical recombination. Optical diagnostics then allow us to track the recombination and cooling that result [6], [7].

The infrared spectral region is of interest because it provides direct measurements of the CO and CO₂ ground state densities and rovibrational population distributions [8]. This work is a continuation of the work presented last year [9], which looked at infrared emission spectra from a CO₂/Ar plasma at the exit of the inductively coupled plasma torch (which corresponds to the inlet of the water-cooled tube test-section). This paper presents our first infrared measurements obtained at the exit of the water-cooled test-section. Our goal is to study the highly resolved emission spectrum to track the thermochemical state of the plasma and to determine a possible departure from equilibrium as previously observed for N₂/Ar mixtures studied using this configuration [6], [10].

¹ Ph.D. Candidate, Laboratoire EM2C, CNRS UPR288, CentraleSupélec, Université Paris Saclay.

² Assistant Professor, Laboratoire EM2C, CNRS UPR288, CentraleSupélec, Université Paris Saclay, AIAA Member

³ Professor, Laboratoire EM2C, CNRS UPR288, CentraleSupélec, Université Paris Saclay, AIAA Fellow.

II. Experimental Setup

The plasma torch facility at the EM2C laboratory produces atmospheric pressure plasmas with temperatures ranging between 6000 and 9000 K depending upon the gas mixture used. The plasma facility is a TAFE Model 66 Inductively Coupled Plasma (ICP) torch powered by a 120 kVA radio frequency LEPEL Model T-50-3 power supply. The torch operates at 4 MHz and can deliver up to 50 kW of power to the plasma. Fig. 1 shows a schematic of the ICP torch. More details of the plasma torch facility may be found in [11], [12]. The CO₂ plasma flow studied here exits the torch through a 1-cm diameter nozzle at a speed between 500 and 700 m/s and is composed of 0.35 g/s ($\pm 2\%$) of carbon dioxide premixed with 3.10 g/s ($\pm 2\%$) of argon to provide stable and sustainable operating conditions. Consequently, the mass fractions of the mixture are respectively 10% for CO₂ and 90% for Ar. The high fraction of argon, easily ionizable, is required to provide stable and sustainable operating conditions. For this injection mixture, approximately 50% of the mixture is injected via the radial injectors and 50% via the swirl injectors. Increasing the swirl injection increases the symmetry of the plasma jet but also reduces the stability of the torch – our choice is a compromise between these competing effects. Finally, the plate power is 45 kW (note that less power is coupled into the plasma). Water-cooled test-sections of various lengths (5, 10, 15, 20, 25, 30 and 35 cm) can be placed on the 1-cm diameter exit of the torch to provoke rapid cooling and therefore force plasma recombination in a well-controlled environment. All emission measurements are made 0.25 cm downstream of the test-section exit (i.e., $D/4$, where D is the diameter of the tube).

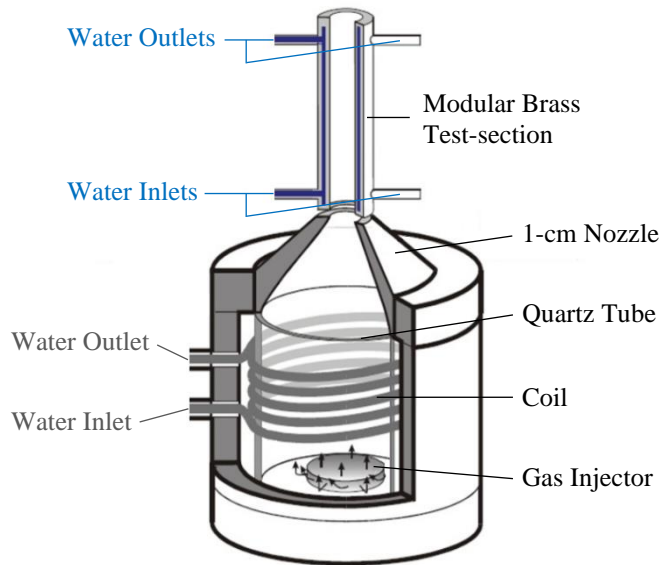


Fig. 1 Schematic of ICP torch head with non-equilibrium test-section for CO₂ recombination experiments.

The infrared OES measurements are performed using a 0.75-m focal length spectrometer (Princeton Instruments Acton SpectraPro 2750i) fitted with a 512x640 pixel cryogenically cooled (liquid N₂) infrared camera (IRcameras IRC-806). To reduce absorption from cold CO₂ and H₂O present in the room, 90% of the optical path is purged with dry N₂. The observed infrared background signal strongly drifts over time. To track and remove this background, a chopper is placed at the entrance to the spectrometer. The background, and the signal coming from the plasma are acquired at 60 Hz. Two parabolic mirrors (focal length of 20 and 50 cm) are used to collect the signal. The spectrometer is fitted with a 300 groove/mm diffraction grating blazed at 4.0 μm and higher order interferences are rejected by using a long-pass filter with cut-off at 3.6 μm (Edmund Optics 68-660). Fig. 2 shows the experimental setup for the infrared OES measurements. The spectra are calibrated in absolute intensity using a tungsten lamp traceable to NIST standards (Optronics Laboratory OL550) equipped with a sapphire window for IR transmittivity. Special attention was paid to accurately calibrate the measurements because cold CO₂ and H₂O present in the optical path absorb the signal in the IR. The complete procedure to remove the absorption effects and correct the calibration is described in Ref. [9], [13].

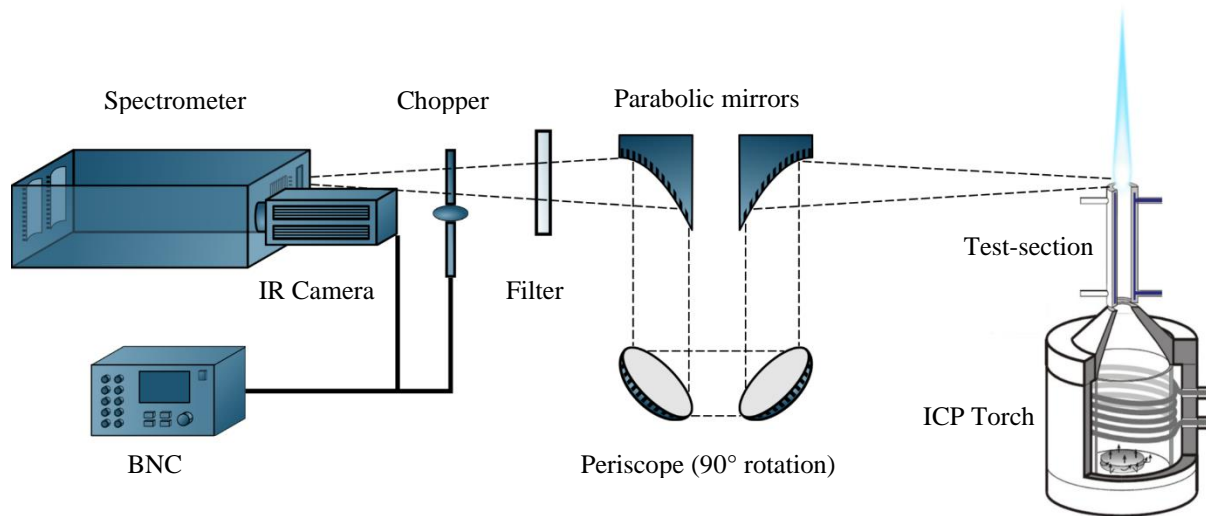


Fig. 2 Schematic of the experimental setup used for IR Optical Emission Spectroscopy (OES).

III. IR OES measurements at the inlet of the water-cooled tube (exit of the torch)

A. Radial symmetry of the profile

Infrared emission measurements, calibrated in absolute intensity, were performed at the exit of the torch from 4150 to 5600 nm. Figure 3 shows the absolute intensity - measured along the line of sight of the spectrometer - as a function of wavelength and radial jet position. A cross-section showing the radial profile is on the right of the figure - this cross-section was obtained by summing the intensity across all wavelengths for a given radial position. It therefore represents an average of the radial profile across all wavelengths. The blue curve represents the measured radial profile. The orange curve is an average between the right and left half-profiles. The good agreement between both curves indicates that the measured profile is indeed symmetric to a high degree of approximation. The absolute intensity of the measured spectral emission is estimated to be accurate within 5% of the reported amplitude. The profile is slightly wider than the diameter of the torch nozzle (1 cm), indicated by the two dashed black lines. The M shape

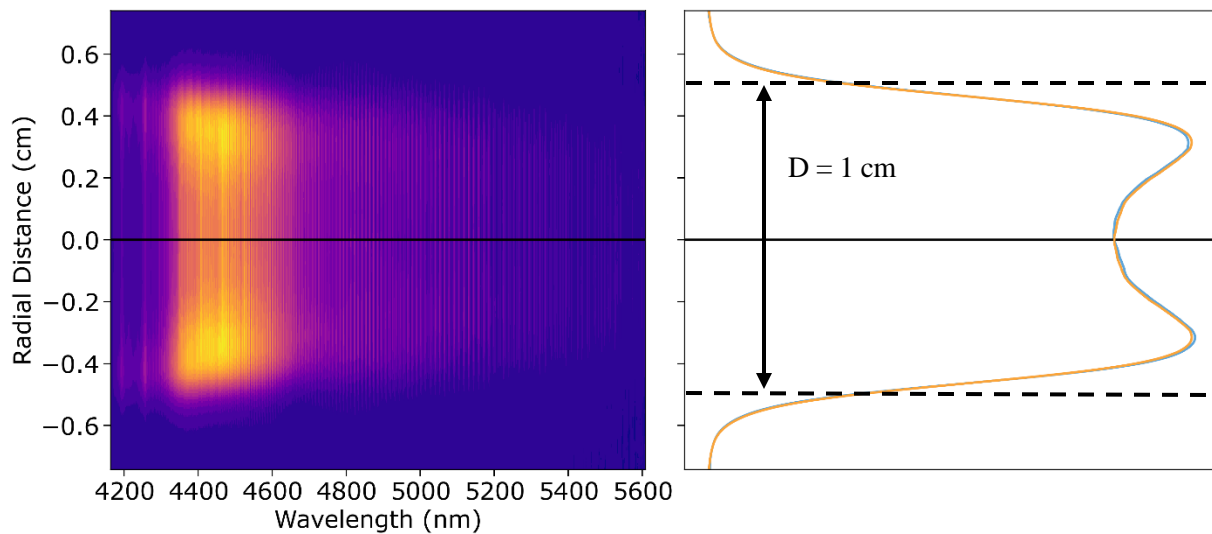


Fig. 3 Absolute intensity measured along the line of sight of the spectrometer on the left. Cross-section obtained by summing the intensity across all wavelengths showing the radial profile on the right, the measured radial profile is in blue and an average between the right and left half-profiles is in orange curve.

of the profile indicates that the edges of the plasma radiate more than the center. The radiation from the central region, where the temperature is about 7000 K, is dominated by CO emission in the range 4.1 - 5.6 μm . The radiation from the edges, where the temperature is colder, is due to CO₂ emission in the same spectral region.

B. Calibrated and abel-inverted spectrum at the exit of the torch

Once calibrated in absolute intensity, the measured spectrum is abel-inverted to obtain the spatially resolved volumetric emission of the plasma. The center of the radial profile is a singular point for the abel-inversion integral and suffers from large uncertainty up to 60% for the worst parts of the spectrum. The uncertainty of the emission coming from the radial position $r = 1$ mm is much less affected by this problem, only 20% for the worst parts of the spectrum. The assumption of cylindrical symmetry – supported by the observed symmetry of the intensity profile – requires that there be no gradients at $r = 0$ mm. Furthermore, the line-of-sight spectra at $r = 0$ mm and $r = 1$ mm are very close, thus indicating that the spectra at $r = 1$ mm is representative of the emission on centerline. Figure 4 shows the emission coming from the $r = 1$ mm radial position. This spectrum from 4290 to 5600 nm is composed entirely of high temperature CO emission. Colder CO₂ present in the optical path absorbs the signal from 4200 to 4350 nm whereas H₂O, due to the humidity of ambient air along the optical path, impacts the spectrum above 5000 nm. The impact of this absorption is significant, even though 90% of the path is purged with dry N₂. To extract parameters such as the temperature and the density of CO, this spectrum is compared against simulations in the next section.

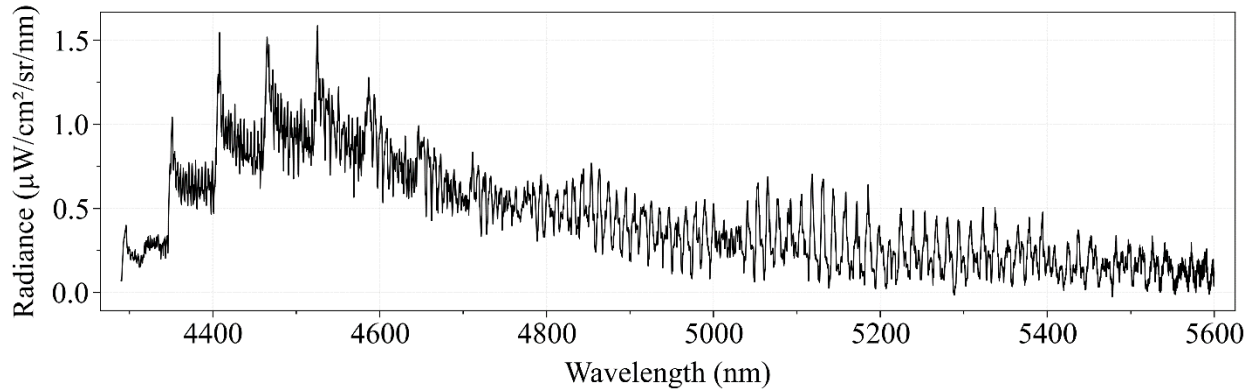


Fig. 4 Calibrated and abel-inverted OES measurements between 4290 and 5600 nm at the inlet of the water-cooled test-section (exit of the torch) at $r = 1$ mm radial position.

C. Comparison to RADIS simulation using HITEMP-2010

Several LTE spectra at different gas temperatures were calculated using the RADIS line-by-line radiative code [14], accelerated with the algorithm described in Ref. [15], in conjunction with the HITEMP-2010 database [16], valid up to 10 000 K for the CO molecule. The RADIS code, an open access software developed at EM2C allows to calculate the emission from all HITRAN and HITEMP species like CO and CO₂. The residual between the measured and computed spectra is determined according to Equation 1. The best fit – or minimum residual - is found for a gas temperature of 6575 K and a CO density of $3.79 \times 10^{22} \text{ m}^{-3}$.

$$Residual(T_{gas}, n_{CO}) = \sqrt{\left(\sum_{\lambda} \left(Experiment(\lambda) - Simulation(T_{gas}, n_{CO}, \lambda)\right)^2\right)} \quad \text{Equation 1}$$

After this initial step, absorption of cold CO₂ and H₂O present in the optical path is calculated at 300 K and added in the line-of-sight of CO emission to match the level observed. The mole fractions of these two molecules present along the optical path are found by minimizing the residual. The best fit is achieved with 165 ppm of CO₂ and 3300 ppm of H₂O over the 3.6-m optical path length. Figure 5 shows the absorption of CO₂ in green and the absorption of H₂O in blue. The final best fit is presented at the bottom of Fig. 5. The overall good agreement confirms that the plasma at the exit of the torch is in LTE at 6575 K. The uncertainty on the temperature has proven to be difficult to calculate. We are currently working on an uncertainty propagation algorithm that will allow us to ascribe an uncertainty to this temperature.

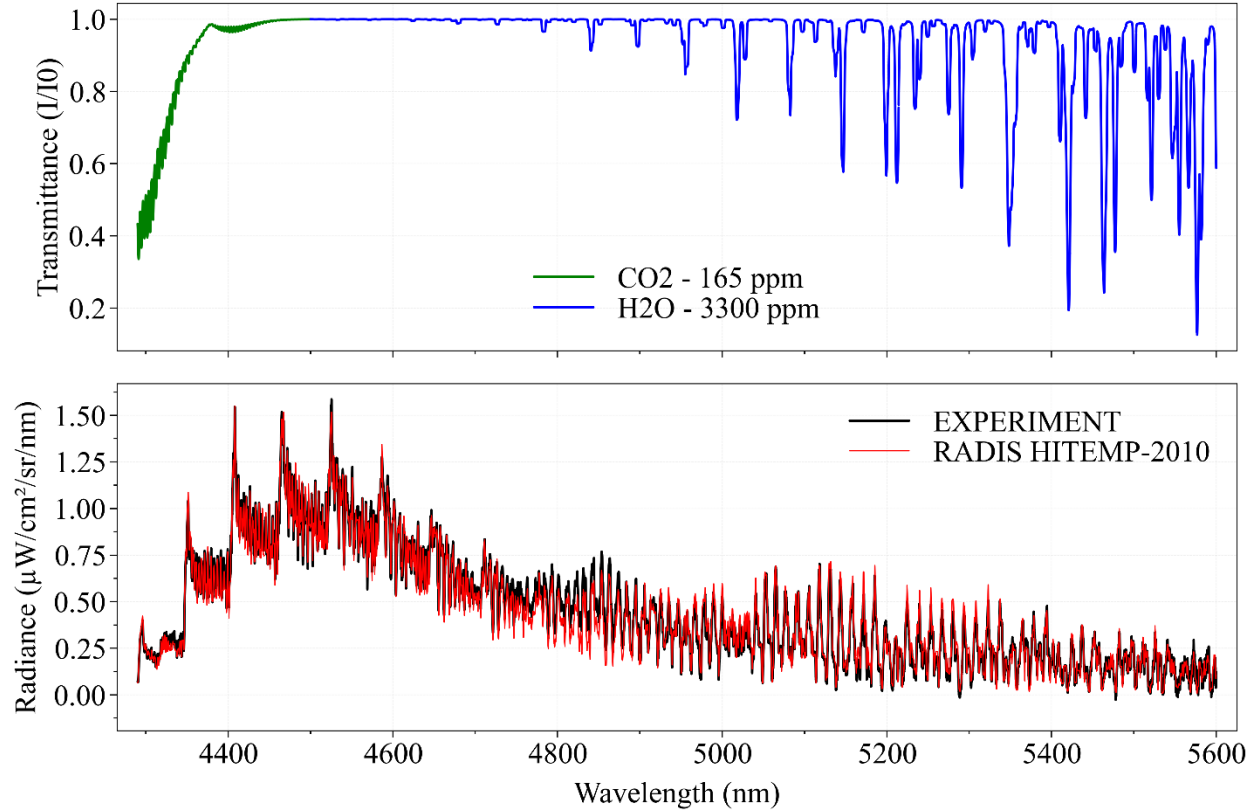


Fig. 5 Comparison between experimental spectrum and RADIS simulation for CO using HITEMP-2010 database between 4290 and 5600 nm at the exit of the torch at $r = 1$ mm radial position. The gas temperature of the simulation is 6575 K, and the CO density is $3.79 \times 10^{22} \text{ m}^{-3}$.

IV. IR OES measurements at the exit of the 35-cm test-section

A. Radiale symmetry of the profile

The IR OES measurements were repeated at the exit of water-cooled test-section of various lengths. We only present here the measurements at the exit of the 35-cm test-section. Figure 6 shows the absolute spectra measured along the line of sight as a function of radial position in the plasma jet. A cross-section showing the radial profile and the mean profile of both sides is on the right of the figure. Once again, the good agreement between both curves indicates that the measured profile is indeed symmetric to a high degree of approximation. As opposed to Fig. 3 where the emission at the center of the jet was observed to be weaker than at its boundaries, here the radial profile is peaked at the center.

B. Calibrated and Abel-inverted spectrum at the exit of the 35-cm test-section

Figure 7 shows the calibrated and Abel-inverted spectrum at the exit of the 35-cm test-section on centerline. Unlike at the inlet of the water-cooled tube, emission from both CO and CO₂ is present on centerline. The emission from these two molecules overlaps one another for a large portion of the observed spectrum. CO₂ emits between 4170 to 4900 nm, with the CO₂ headband visible at 4170.5 nm. CO emits between 4290 to 5600 nm. Absorption from cold room CO₂ is clearly visible from the characteristic lobes between 4200 and 4350 nm. Absorption from cold room H₂O impacts the spectrum in a more subtle manner, affecting a few lines above 5000 nm. The largest impact of cold room H₂O absorption is around 5200 nm.

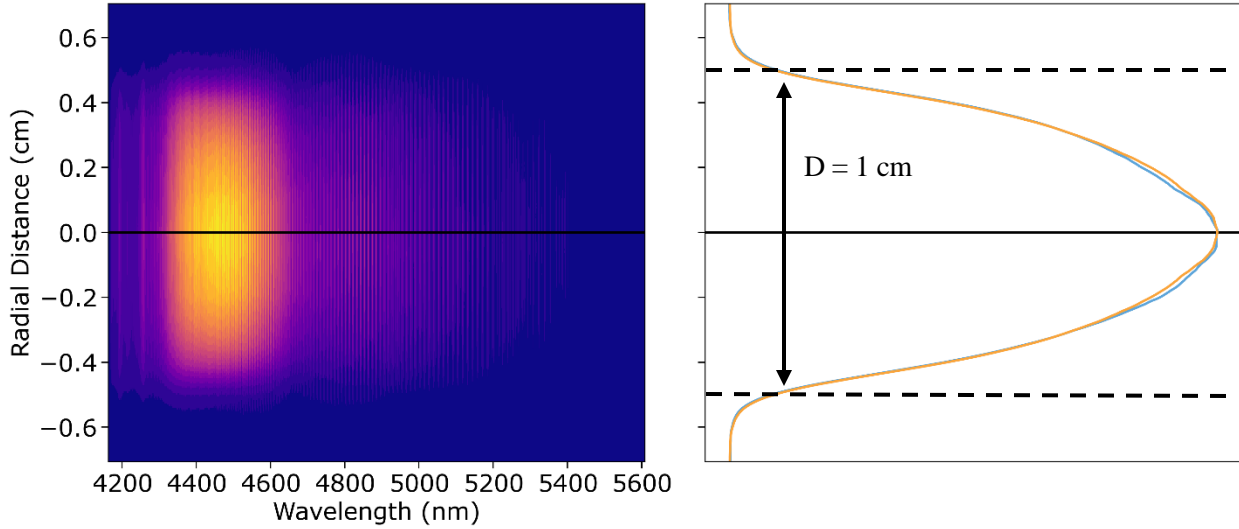


Fig. 7 Absolute intensity measured along the line of sight of the spectrometer on the left. Cross-section obtained by summing the intensity across all wavelengths showing the radial profile on the right, the measured radial profile is in blue an average between the right and left half-profiles is in orange curve.

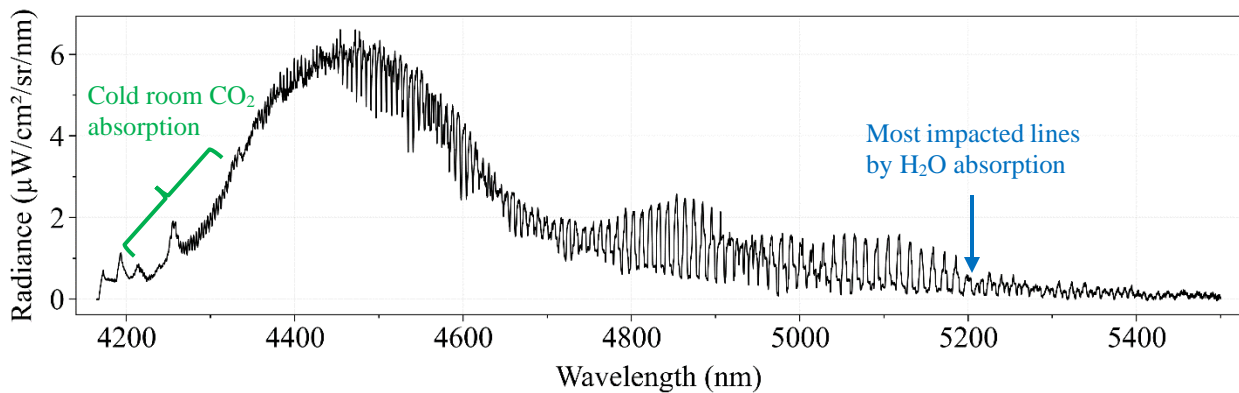


Fig. 6 Calibrated and Abel-inverted OES measurements between 4165 and 5500 nm at the exit of the 35-cm test-section at $r = 0$ mm radial position.

C. CO spectral simulation

The spectral fitting procedure at the exit of the 35-cm test-section differs from the one at the exit of the torch because of the presence of both CO and CO_2 features in the total spectrum. First, we fit the CO spectrum by minimizing the residual (Equation 1) and varying T_{gas} and n_{CO} . It should be noted that we consider the gas to be in equilibrium for this fit - i.e., $T_{gas} = T_{vib} = T_{rot}$. As a first step in the fitting routine procedure, the residual is only calculated at wavelengths between 5000 – 5500 nm where the spectrum is not impacted by CO_2 . Figure 8 shows the resulting comparison between the measured spectrum in black and the best fit calculated with RADIS using the CO HITEMP-2010 database in red [14], [16]. The best fit yields a temperature of 3000 K and CO density of $1.54 \times 10^{23} \text{ m}^{-3}$. For the simulated spectrum, 3200 ppm of cold H_2O over a 3.6 m optical path was added along the line of sight as described above to match the level observed. Good agreement is found at wavelengths above 5000 nm where CO_2 does not emit. Below 5000 nm, the difference between the measurement and the simulation is due to the contribution of CO_2 which is responsible for approximately half of the total observed emission. The next section will focus on modeling this portion of the emission.

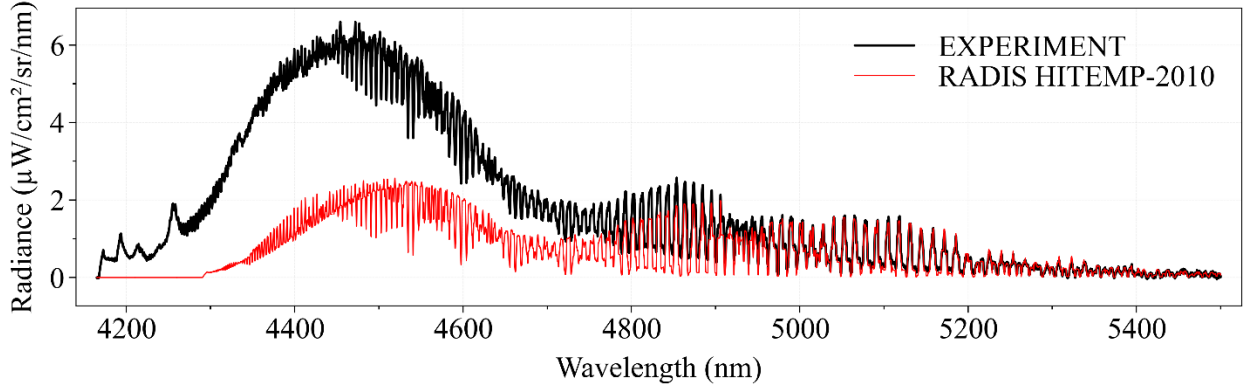


Fig. 8 Comparison between experimental spectrum and RADIS simulation for CO using HITEMP-2010 database between 4165 and 5500 nm at the exit of the 35-cm-test-section. The gas temperature of the simulation is 3000 K, and the CO density is $1.54 \times 10^{23} \text{ m}^{-3}$.

D. CO₂ spectral simulation

The study of the CO₂ headband between 4165 and 4190 nm to determine with great accuracy the rotational temperature of the gas [14]. This region of the spectrum is also unaffected by emission from CO. The best fit obtained by minimizing the residual across this limited wavelength range was achieved for a rotational temperature of 2450 K and a CO₂ density of $3.19 \times 10^{22} \text{ m}^{-3}$, which is 6 times lower than the equilibrium value ($2.11 \times 10^{23} \text{ m}^{-3}$) at 2450 K as calculated using the NASA CEA [17] or Cantera code [18]. In other words, the CO₂ is underpopulated with respect to its equilibrium value. Figure 9 shows the comparison between the measured spectrum in black and the RADIS simulation using the CO₂ HITEMP-2010 database over the CO₂ headband. 160 ppm of cold CO₂ over 3.6 m were added in the line of sight to match the absorption observed between 4200 and 4350 nm. Good agreement is observed for the CO₂ headband and above 4800 nm where CO₂ emission is negligible. However, between 4400 and 4800 nm there is a poor agreement between our measurement and the simulation.

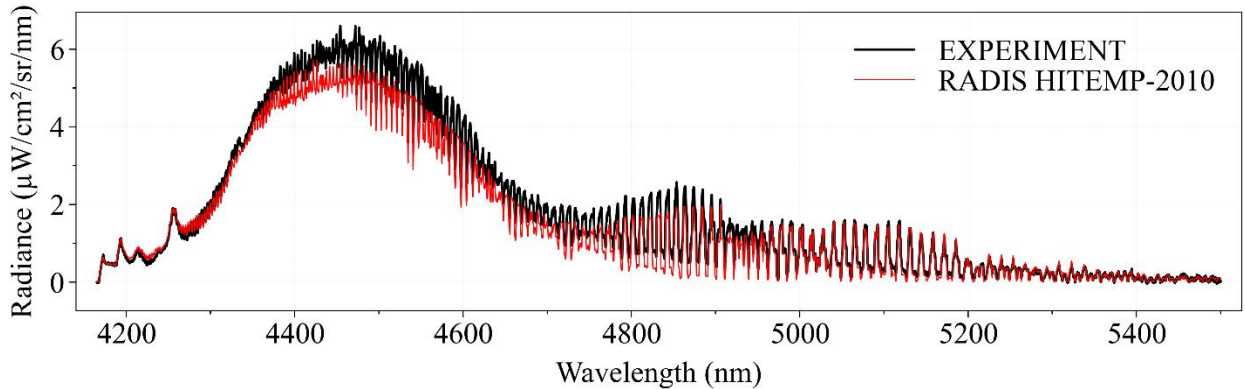


Fig. 9 Comparison between experimental spectrum and RADIS simulation for CO and CO₂ using HITEMP-2010 database between 4165 and 5500 nm at the exit of the 35-cm-test-section. $T_{gas}(CO) = 3000 \text{ K}$; $T_{gas}(CO_2) = 2450 \text{ K}$; $n_{CO} = 1.54 \times 10^{23} \text{ m}^{-3}$; $n_{CO_2} = 3.19 \times 10^{22} \text{ m}^{-3}$.

To improve the agreement between the RADIS calculation and the observed spectrum, we increased the CO₂ vibrational temperature to $T_{vib} = 2600 \text{ K}$ ($T_{vib} = T_{rot} + 150 \text{ K}$). Figure 10 shows the resulting agreement. Note that the HITEMP-2010 database is still valid at this temperature and up to 3000 K for the CO₂ molecule. The agreement with the experimental spectrum at wavelengths above 4300 nm is better assuming this higher vibrational temperature. This augmented vibrational temperature and the CO₂ underpopulation suggest a departure from equilibrium. As before, we note that the uncertainty assessment has not yet been performed on these best-fit parameters. We are currently working on determining this uncertainty.

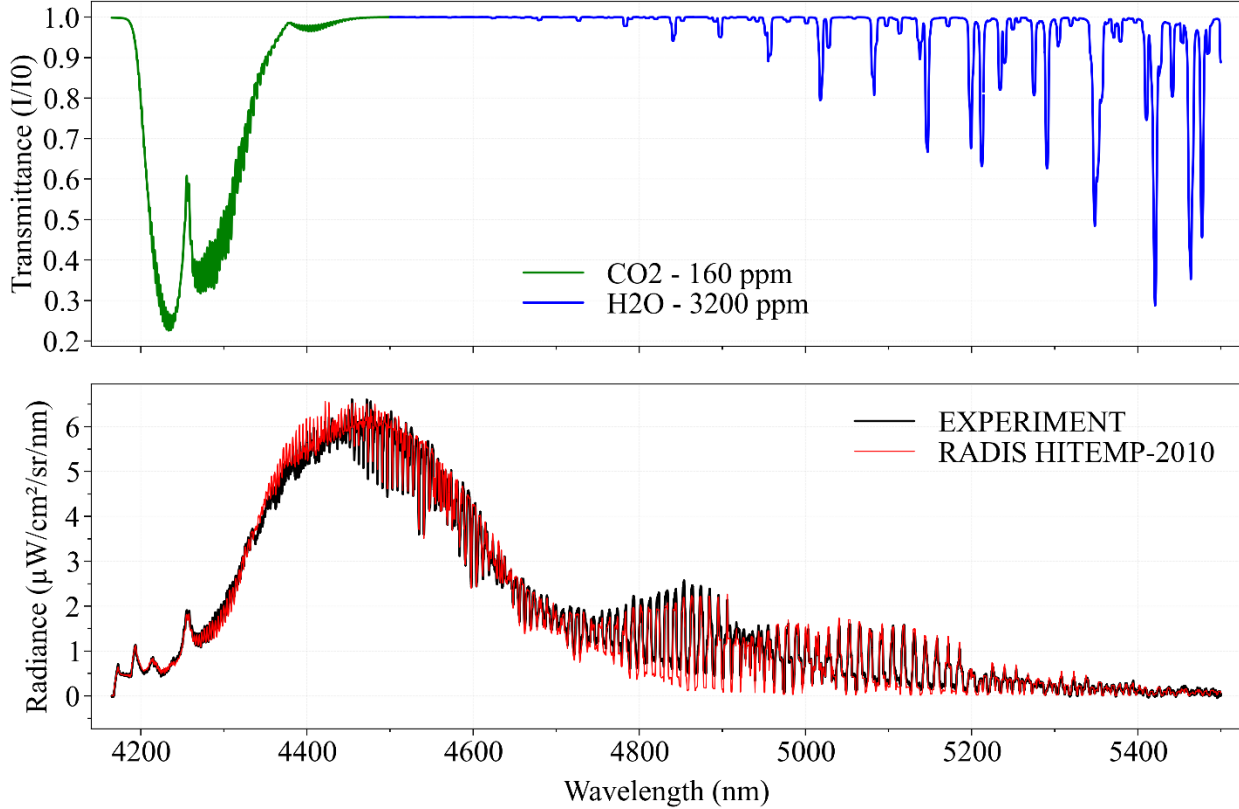


Fig. 10 Comparison between experimental spectrum and RADIS simulation for CO and CO₂ using HITEMP-2010 database between 4165 and 5500 nm at the exit of the 35-cm-test-section. $T_{gas}(CO) = 3000$ K ; $T_{rot}(CO_2) = 2450$ K ; $T_{vib}(CO_2) = 2600$ K ; $n_{CO} = 1.54 \times 10^{23} \text{ m}^{-3}$; $n_{CO_2} = 3.39 \times 10^{22} \text{ m}^{-3}$.

Once the CO₂ parameters are found, the CO parameters are adjusted by considering the full wavelength range of the spectrum for the residual minimization. These steps are repeated until convergence of all parameters for CO and CO₂, typically obtained after 2 or 3 loops. Table 1 summarize all the parameters determined for the final best-fit at the inlet and exit of the 35-cm water-cooled test-section. We draw attention to two observations. First, the rotational temperature of CO is different from the rotational temperature of CO₂. At the moment, because we have not yet performed the uncertainty analysis, it is unclear if this difference is real or could be explained by the uncertainty on each measurement. Second, the rotational temperature of CO₂ is lower than the vibrational temperature of CO₂. While the uncertainty analysis has not yet been done, we see by comparing the spectral fits in Figs: 9 and 10, that this difference appears significant and not due to the uncertainty.

Table 1 Summary of temperatures and densities determined for CO and CO₂ at the inlet and the exit of the 35-cm test-section.

	CO		CO ₂		
	T _{gas} (K)	n (m ⁻³)	T _{rot} (K)	T _{vib} (K)	n (m ⁻³)
Inlet	6575	3.79x10 ²²			
Exit	2875	1.80x10 ²³	2450	2600	3.39x10 ²²

V. 0D simulation with the Park 1995 model using Cantera

A 0D chemical kinetic simulation was realized using the Cantera code [18] in conjunction with the Park 1995 kinetics model [19]. The temperature, as measured above using the CO molecular band, was converted into a time-dependent temperature profile by using estimates of the gas velocity. These velocity estimates rely on 1) an assumption that the velocity profile is self-similar to the temperature profile and 2) knowledge of the total mass passing through the test-section which is known. The time-dependent temperature profile is input into Cantera which then calculates

the evolution of the chemical composition. As an initial condition, the measured chemical composition at the water-cooled tube inlet was used (see section III) and an exponentially decreasing temperature profile matching the temperature found at the exit of the 35-cm test-section. Figure 11 shows the evolution of the major species densities along the axial position of the water-cooled tube. CO and CO₂ densities are respectively in orange and green. CO density prediction at 35 cm is in good agreement with our measurement at the exit of the 35-cm test-section. However, the CO₂ density is underpredicted by a factor of about 10. These initial results should be interpreted with care given that we have not yet performed the uncertainty analysis for the measurements. Part of the factor 10 discrepancy may also be related to our simplifying assumption of an exponentially decaying temperature profile between 0 and 35 cm. Measurements at intermediate positions, every 5 cm, will help us refine this time-temperature history.

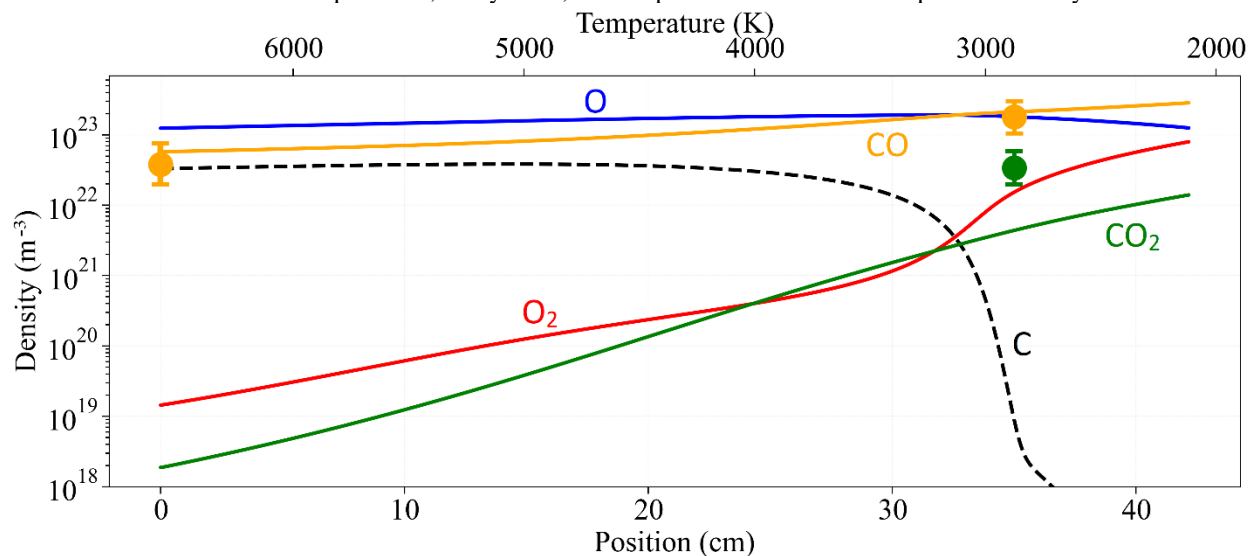


Fig. 11 0D simulation with the Park 1995 kinetics model using the Cantera code between the inlet and outlet of the water-cooled test-section. CO and CO₂ densities are respectively in orange and green.

VI. Conclusion and Future work

We present infrared optical emission measurements from a recombining high temperature CO₂/Ar plasma jet at the inlet and exit of a 35-cm water-cooled test section. These measurements are calibrated in absolute intensity and Abel-inverted to provide the spatially resolved volumetric emission. The resulting spectra are compared to simulations made with the line-by-line radiative code RADIS in conjunction with the HITEMP-2010 database [14], [16]. High quality fits indicate a temperature of 6650 K at the water-cooled tube inlet. The measurements and analysis at the exit of the water-cooled tube suggest a departure from equilibrium (chemical and vibrational). An initial 0D simulation was performed using the measured temperature profile and the Park 1995 chemical-kinetic model with the Cantera code [17], [18]. Good agreement was observed for the predicted density of CO, but CO₂ was underpredicted by a factor of about 10.

We are currently working to assess the uncertainty on the measured temperatures and densities. This will enable us to fully characterize the thermochemical state of the plasma as a function of radial position in the plasma jet and as a function of test section length. The same measurements reported here were performed at the exit of water-cooled test sections of lengths varying between 5-cm and 30-cm. Our goal is to track the thermochemical state of the plasma and to observe what happens as the plasma is continuously cooled. The axial centerline temperature profile will be then used to perform 0D simulations using Park and Cruden chemical-kinetic models [19], [20]. To complete this dataset, power balance measurements will also be performed. For these, the water temperatures at the inlet and outlet of the water-cooled tube were measured and will be used to determine the enthalpy removed from the plasma. The measured drop in enthalpy can then be compared with calculations based on the thermochemical state of the plasma at the inlet and exit of the water-cooled tube as a consistency check.

Acknowledgments

This work is financially supported by the CO2REC grant (Number: ANR-18-CE05-0003) from the Agence Nationale de la Recherche (ANR).

The authors would like to thank Dr. Erwan Pannier for his help with the RADIS analyses.

References

- [1] I. Cozmuta, M. J. Wright, B. Laub, and W. H. Willcockson, "Defining ablative thermal protection system margins for planetary entry vehicles," *42nd AIAA Thermophys. Conf.*, no. June, pp. 1–27, 2011, doi: 10.2514/6.2011-3757.
- [2] Dr. David R. Williams, "Mars Fact Sheet," 2018. <https://nssdc.gsfc.nasa.gov/planetary/factsheet/marsfact.html> (accessed Oct. 01, 2019).
- [3] C. O. Johnston, A. M. Brandis, and K. Sutton, "Shock layer radiation modeling and uncertainty for mars entry," *43rd AIAA Thermophys. Conf. 2012*, no. June, pp. 1–43, 2012, doi: 10.2514/6.2012-2866.
- [4] C. O. Johnston and M. Panesi, "Advancements in afterbody radiative heating simulations for earth entry," *46th AIAA Thermophys. Conf.*, no. June, pp. 1–19, 2016, doi: 10.2514/6.2016-3693.
- [5] J. Annaloro, A. Bultel, and P. Omaly, "Detailed kinetic of CO₂ dissociation and C ionization: Application to atmospheric Martian entries," *J. Phys. Conf. Ser.*, vol. 511, no. 1, 2014, doi: 10.1088/1742-6596/511/1/012053.
- [6] C. O. Laux, L. Pierrot, and R. J. Gessman, "State-to-state modeling of a recombining nitrogen plasma experiment," *Chem. Phys.*, vol. 398, no. 1, pp. 46–55, 2012, doi: 10.1016/j.chemphys.2011.10.028.
- [7] A. Tibère-Inglesse, S. McGuire, and C. O. Laux, "Nonequilibrium radiation from a recombining nitrogen plasma," *AIAA Aerosp. Sci. Meet. 2018*, no. 210059, 2018, doi: 10.2514/6.2018-0241.
- [8] S. D. McGuire, A. C. Tibère-Inglesse, and C. O. Laux, "Infrared spectroscopic measurements of carbon monoxide within a high temperature ablative boundary layer," *J. Phys. D. Appl. Phys.*, vol. 49, no. 48, 2016, doi: 10.1088/0022-3727/49/48/485502.
- [9] C. H. C. Grimaldi, S. D. McGuire, A. Tibère-Inglesse, and C. O. Laux, "Infrared radiation measurements of a recombining co₂ plasma at atmospheric pressure," *AIAA Scitech 2021 Forum*, pp. 1–14, 2021, doi: 10.2514/6.2021-0104.
- [10] A. Tibère-inglesse, "Radiation of nonequilibrium recombining plasma flows," p. 233, 2019, [Online]. Available: <https://tel.archives-ouvertes.fr/tel-02454286/document%0Ahttps://tel.archives-ouvertes.fr/tel-02454286>.
- [11] C. O. Laux, T. G. Spence, C. H. Kruger, and R. N. Zare, "Optical diagnostics of atmospheric pressure air plasmas--- Stanford University.pdf," vol. 12, pp. 125–138, 2003.
- [12] M. E. MacDonald, C. M. Jacobs, C. O. Laux, F. Zander, and R. G. Morgan, "Measurements of air plasma/ablator interactions in an inductively coupled plasma torch," *J. Thermophys. Heat Transf.*, vol. 29, no. 1, pp. 12–23, 2015, doi: 10.2514/1.T4402.
- [13] D. Packan, C. O. Laux, R. J. Gessman, L. Pierrot, and C. H. Kruger, "Measurement and modeling of OH, NO, and CO₂ infrared radiation at 3400 K," *J. Thermophys. Heat Transf.*, vol. 17, no. 4, pp. 450–456, 2003, doi: 10.2514/2.6803.
- [14] E. Pannier and C. O. Laux, "RADIS: A nonequilibrium line-by-line radiative code for CO₂ and HITRAN-like database species," *J. Quant. Spectrosc. Radiat. Transf.*, vol. 222–223, pp. 12–25, 2019, doi: 10.1016/j.jqsrt.2018.09.027.
- [15] D. C. M. van den Bekerom and E. Pannier, "A discrete integral transform for rapid spectral synthesis," *J. Quant. Spectrosc. Radiat. Transf.*, vol. 261, p. 107476, Mar. 2021, doi: 10.1016/j.jqsrt.2020.107476.
- [16] L. S. Rothman *et al.*, "HITEMP, the high-temperature molecular spectroscopic database," *J. Quant. Spectrosc. Radiat. Transf.*, vol. 111, no. 15, pp. 2139–2150, 2010, doi: 10.1016/j.jqsrt.2010.05.001.
- [17] B. J. McBride, *Computer Program for Calculation of Complex Chemical Equilibrium Compositions and Applications*. NASA, 1996.
- [18] D. G. Goodwin, R. L. Speth, H. K. Moffat, and B. W. Weber, "Cantera: An object-oriented software toolkit for chemical kinetics, thermodynamics, and transport processes," 2021, doi: 10.5281/zenodo.4527812.
- [19] C. Park, J. T. Howe, R. L. Jaffe, and G. V. Candler, "Review of chemical-kinetic problems of future NASA missions, II: Mars entries," *J. Thermophys. Heat Transf.*, vol. 8, no. 1, pp. 9–23, 1994, doi: 10.2514/3.496.
- [20] B. A. Cruden, A. M. Brandis, and M. E. Macdonald, "Characterization of CO thermochemistry in incident shockwaves," *2018 Jt. Thermophys. Heat Transf. Conf.*, pp. 1–22, 2018, doi: 10.2514/6.2018-3768.